# Spin-Based Diagnostic of Nanostructure in Copper Phthalocyanine–$C_{60}$ Solar Cell Blends

**Marc Warner,[†,*] Soumaya Mauthoor,[‡] Solveig Felton,[‡] Wei Wu,[†,‡,§] Jules A. Gardener,[†,∥] Salahud Din,[‡] Daniel Klose,[⊥,¶] Gavin W. Morley,[†] A. Marshall Stoneham,[†] Andrew J. Fisher,[†] Gabriel Aeppli,[†] Christopher W. M. Kay,[⊥,*] and Sandrine Heutz[‡,*]**

[†]London Centre for Nanotechnology and Department of Physics and Astronomy, University College London, London WC1H 0AH, U.K., [‡]London Centre for Nanotechnology and Department of Materials and [§]Department of Chemistry and London Centre for Nanotechnology, Imperial College London, London SW7 2AZ, U.K., and [⊥]Institute of Structural & Molecular Biology and London Centre for Nanotechnology, University College London, London WC1E 6BT, U.K. [∥]Present address: Physics Department, Harvard University, Cambridge, MA 02138. [¶]Present address: University of Osnabrück, Department of Physics, Barbarastrasse 7, 49076 Osnabrück, Germany.

**ABSTRACT** Nanostructure and molecular orientation play a crucial role in determining the functionality of organic thin films. In practical devices, such as organic solar cells consisting of donor–acceptor mixtures, crystallinity is poor and these qualities cannot be readily determined by conventional diffraction techniques, while common microscopy only reveals surface morphology. Using a simple nondestructive technique, namely, continuous-wave electron paramagnetic resonance spectroscopy, which exploits the well-understood angular dependence of the *g*-factor and hyperfine tensors, we show that in the solar cell blend of $C_{60}$ and copper phthalocyanine (CuPc)—for which X-ray diffraction gives no information—the CuPc, and by implication the $C_{60}$, molecules form nanoclusters, with the planes of the CuPc molecules oriented perpendicular to the film surface. This information demonstrates that the current nanostructure in CuPc:$C_{60}$ solar cells is far from optimal and suggests that their efficiency could be considerably increased by alternative film growth algorithms.

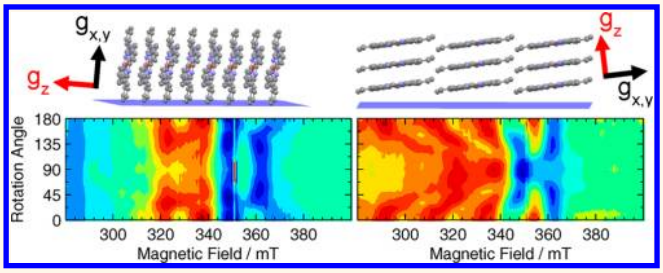


**KEYWORDS:** EPR · organic solar cells · molecular aggregation · molecular orientation · DFT · XRD · texture analysis

The physical properties[1−5] and functionality of organic thin films strongly depend on nanostructure and molecular orientation. In particular, texturing, where the preferential orientation of crystallites is engineered to improve charge transport[6,7] and blending,[8−10] enhance the performance of optoelectronic devices such as organic solar cells. For solar cells based on copper phthalocyanine (CuPc, Figure 1a) and $C_{60}$, increasing control over the device structure, for example, combining blends with continuous layers in tandem structures, has improved efficiency from ∼1% up to ∼5.7%.[11] The simplest film architecture relies on layers of CuPc and $C_{60}$ stacked on top of each other, as illustrated in Figure 1b, a structure referred to as a "bilayer". When the CuPc film is deposited onto the electrode using vacuum deposition, XRD shows that it crystallizes in the α-phase, in which the molecules are nearly perpendicular to the substrate and form columns with the stacking axis parallel to the substrate.[6] Therefore, the direction of maximum charge transport is parallel to the electrodes, which is not ideal for optimized efficiency.[6] Furthermore, the CuPc–$C_{60}$ interfacial area where exciton separation into useful charge carriers occurs is restricted to the planar interface. Nanostructured or blended films, depicted schematically in Figure 1c, improve exciton separation, with concomitant gains in efficiency.[8,10,12,13] Although in some cases the blend produces CuPc nanocrystals similar to those in single layers,[10] other reports highlight the disappearance of crystalline order.[8,13,14] It is therefore unclear whether device improvement is due to either blending or changes in molecular orientation or both.

Nondestructive characterization of such complex nanostructures is essential for both fundamental understanding and quality control but cannot be performed by standard

* Address correspondence to marc.warner@ucl.ac.uk, c.kay@ucl.ac.uk, s.heutz@imperial.ac.uk.

Received for review September 9, 2012 and accepted November 18, 2012.

**Published online November 27, 2012**
**10.1021/nn304156e**

methods, instead requiring difficult sample preparation and/or large-scale facilities such as synchrotrons. Various techniques have been used to study molecular orientation in organic semiconductor films. For crystalline samples, X-ray diffraction (XRD) can reveal the structure and texture of films, from which orientation can be derived. However, for amorphous samples or those with grain sizes smaller than ~10 nm, XRD is uninformative. Methods that do not rely on crystallinity include near-edge X-ray absorption fine structure (NEXAFS)[15,16] and, more recently, polarized X-ray scattering,[17] both requiring synchrotron radiation, or optical spectroscopy.[3,18,19] The latter requires detailed prior knowledge of optical properties, while analysis of mixtures is complex and does not provide straightforward information about nearest-neighbor occupancy.

In contrast, electron paramagnetic resonance (EPR) spectroscopy can be used to determine both molecular orientation and clustering within samples that do not exhibit any crystalline order and has been applied to polymers[20,21] and CuPc films.[22] Assessing the molecular orientation relies on anisotropic contributions to the spin Hamiltonian from the electronic Zeeman ($g$) interaction and the hyperfine ($A$) coupling, while line broadening with respect to isolated CuPc molecules, due to the exchange interaction, reveals the extent of clustering. Here we use EPR spectroscopy to determine both the orientation and molecular clustering in the important solar cell blend of $C_{60}$ and CuPc—for which X-ray diffraction gives no information.

## RESULTS

We examined two 200 nm thick films of a CuPc:$C_{60}$ mixture obtained by coevaporation of 50% CuPc and 50% $C_{60}$ (hereafter labeled CuPc:$C_{60}$) either directly onto Kapton or onto a 20 nm thick $H_2$Pc layer on Kapton which emulate improved photovoltaic structures.[8,13] These films lack a pronounced grain structure (Figure 2a), and the surface roughness is 1 order of magnitude lower than for pure Pc films (Figure 2b), as used in bilayers. The XRD data from the two CuPc:$C_{60}$ films are either featureless or show only one peak which corresponds to the 20 nm thick $H_2$Pc, indicating that if the blends contain a significant proportion of crystallites, then their diameters must be below 20 nm (Figure 3a,b). The failure of XRD to yield orientation information for the mixed films necessitates the use of another technique, and the unpaired electron on the copper $d_{x^2-y^2}$ orbital allows CuPc to be studied *via* EPR spectroscopy.[23]

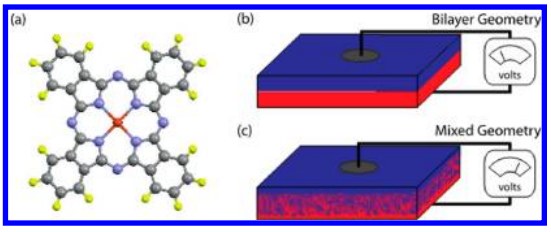


**Figure 1. (a) Molecular structure of CuPc. Yellow, grey, blue and red spheres represent H, C, N and Cu atoms. Schematic of heterojunction solar cells showing both (b) bilayer and (c) blended geometries.**

Here we probe the molecular orientation of these thin films of CuPc by exploiting the angular dependence of the EPR spectrum of a CuPc molecule and the aggregation of CuPc in mixed films by its effect on the EPR spectral line width. Figure 3c,d shows the extrema in angular variation of the EPR spectra of the CuPc:$C_{60}$ films. Because there are many terms in the spin Hamiltonian that, depending on the relative interaction strengths, can have similar effects, interpretation of a single spectrum is difficult. To establish that the spectral shape is the result of molecular orientation, it is necessary to perform EPR as the sample is rotated with respect to the magnetic field; panels e and f of Figure 3 are contour representations of the resulting rotation patterns. They straightforwardly demonstrate that EPR can provide information where XRD cannot. Further details about the spectral features are given below.

To further our understanding of the system, we compare the CuPc:$C_{60}$ film with a judiciously chosen model system, CuPc:$H_2$Pc mixtures, where we can control the nanostructure directly through deposition conditions. It is known that CuPc can be cosublimed with $H_2$Pc (which is diamagnetic) to form spin-diluted mixtures,[24] where the reduced spin−spin interactions increase spectral resolution.[25] Dilution-dependent changes are mainly due to dipolar broadening and exchange narrowing.[26,27] Molecular orientation can be controlled through an intermediate layer of

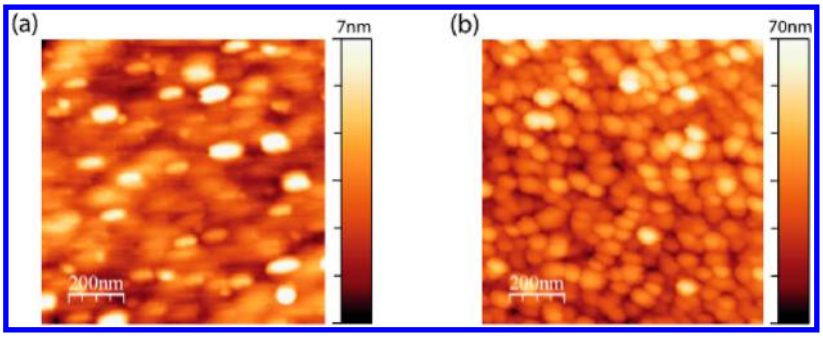


**Figure 2. AFM images of (a) CuPc:$C_{60}$ film and (b) templated 5% CuPc:$H_2$Pc film. Note the difference in vertical scale.**

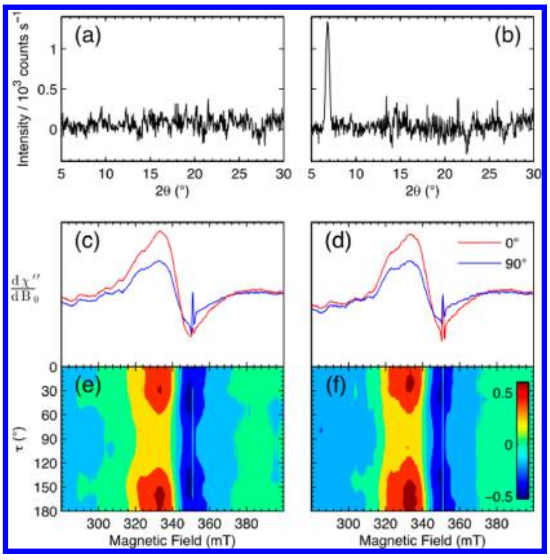


**Figure 3. XRD patterns of (a) CuPc:$C_{60}$ film and (b) CuPc:$C_{60}$ on 20 nm $H_2$Pc. EPR spectra of (c) CuPc:$C_{60}$ film and (d) CuPc:$C_{60}$ on 20 nm $H_2$Pc at both 0 and at 90° with respect to the applied magnetic field. Contour maps showing the orientation dependence of EPR spectra on a (e) CuPc:$C_{60}$ film and (f) CuPc:$C_{60}$ on 20 nm $H_2$Pc.**

perylene-3,4,9,20-tetracarboxylic dianhydride (PTCDA) between CuPc and the substrate. This has been shown to modify the orientation of CuPc molecules through templating,[6] forcing the molecular plane to lie parallel to the substrate, rather than in the nearly perpendicular orientation found if no PTCDA is present on an amorphous substrate such as Kapton.[28]

Figure 4 (left panel) shows fingerprints for four films with known molecular orientation and spin dilution that were obtained by plotting the rotation data as contour maps, alongside simulations (Figure 4, right panel) for the distribution of molecular orientation as determined from XRD (see below and Figure 6), taking into account both the mean molecular orientation and the spread.

The EPR spectrum is due to a spin 1/2 electron on the copper. The CuPc molecule has axial symmetry in both the *g* factor and the copper hyperfine coupling,[25] and the values of *g* are different in the plane of the molecule and along the molecular axis. The large splittings observed are due to the hyperfine interaction with the copper nuclear spin of 3/2, which is also axially symmetric, and leading to four peaks for each value of *g*. The peaks are broadened by the presence of two copper isotopes (69% $^{63}$Cu and 31% $^{65}$Cu) both with the same nuclear spin of 3/2 but with slightly different gyromagnetic ratios (1.484 and 1.588, respectively) and further split by an interaction with the four identical nitrogen atoms, which leads to each copper peak being subdivided into 9. The spectra are broadened by the spin−spin interactions between copper atoms on neighboring molecules, so this hyperfine structure is not observed for pure and lightly diluted CuPc. However, it does

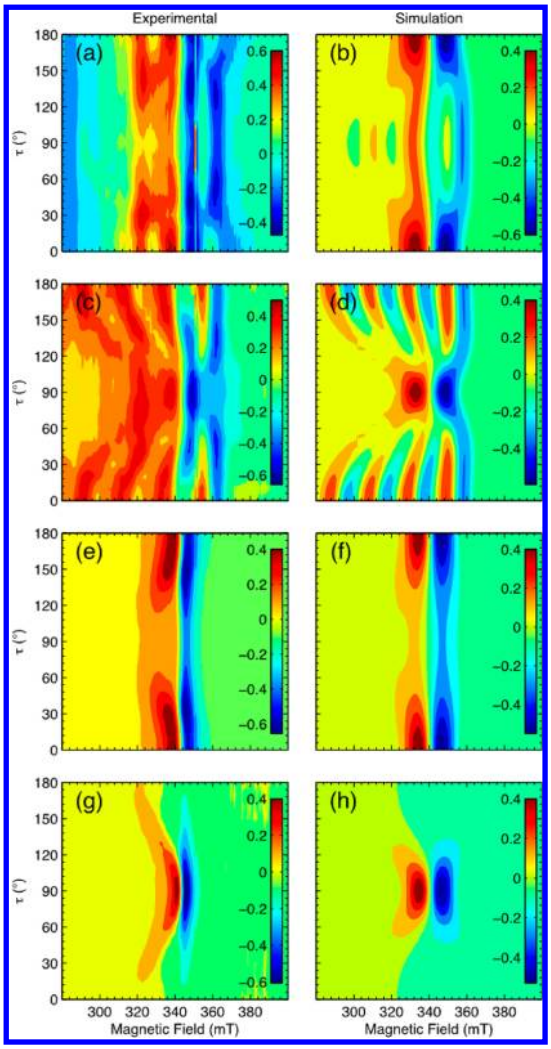


**Figure 4. Contour maps showing the orientation dependence of EPR spectra for CuPc. The left-hand column shows experimental spectra for 200 nm thickness films of (a) 50% CuPc:$H_2$Pc, (c) 50% CuPc:$H_2$Pc on 20 nm PTCDA, (e) 100% CuPc on Kapton, and (g) 100% CuPc on 20 nm PTCDA. The right-hand column shows simulated spectra for CuPc with molecular distributions as determined from XRD: (b,d) no exchange interaction with distributions as for a film without PTCDA and a film with PTCDA, respectively; (f,h) exchange interaction of 1K with distributions as for a film without PTCDA and a film with PTCDA, respectively.**

become visible when the CuPc is diluted down to approximately 5% in $H_2$Pc, as shown in Figure 5. Hence, for the dilute samples, the simulations do not need to take into account neighboring copper atoms and are therefore also faster.

The simulations are performed with the known *g* and $A_{Cu}$ values[25] ($g_\perp$ = 2.0390, $g_\parallel$ = 2.1577, $A_\perp$ = −83 MHz, and $A_\parallel$ = −648 MHz, with subscripts ⊥ and || referring to the direction parallel and perpendicular to the molecular plane, respectively;[25] see Materials and Methods section for further details) with and without an exchange interaction; the line width of the copper hyperfine splitting is adjusted to match the experimental data. The inclusion of an exchange interaction

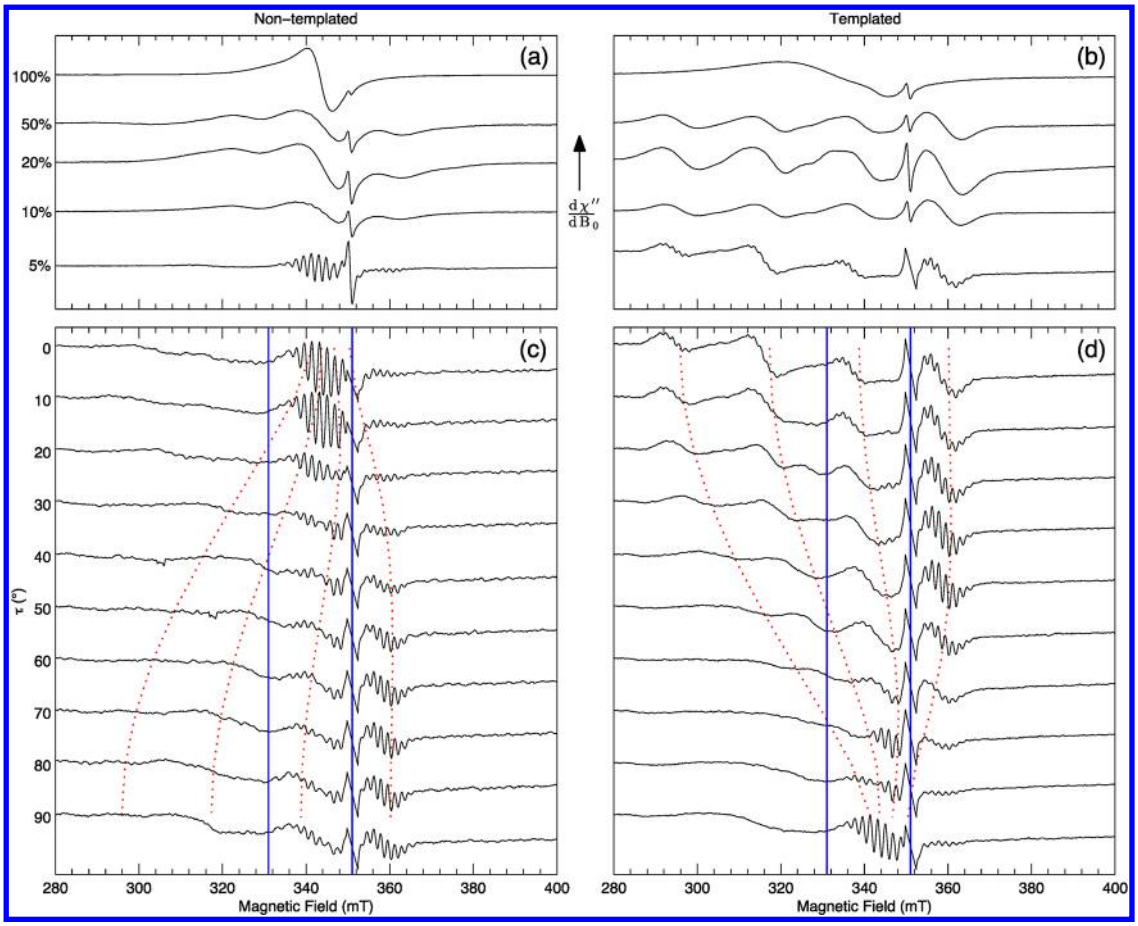


**Figure 5. EPR spectra of thin films of copper phthalocyanine; the left- and right-hand columns depict nontemplated and templated data respectively. (a,b) Variation in line width of both films at differing spin concentrations, which are specified to the left of the graph in (a). Note that the films are perpendicular to the magnetic field; *i.e.*, $\tau = 0°$. Angular variation of the EPR spectra for (c) nontemplated 5% CuPc:$H_2$Pc and (d) templated 5% CuPc:$H_2$Pc; the red dashed curves are a guide for the eye depicting the angular variation of *g*-factor and copper hyperfine interaction for a single molecular orientation; the blue vertical lines designate two standard deviations of the Gaussian wavelet transform used in the sharpness measure. In all spectra, Kapton peaks at ~350 mT have been reduced for ease of viewing.**

reproduces the coalescence of the copper hyperfine structure observed on going from 50% CuPc:50% $H_2$Pc (hereafter abbreviated as 50% CuPc:$H_2$Pc) to 100% CuPc. The contour maps of the experimental spectra for the four samples are distinct and are excellently reproduced by the simulations. Thus we have generated four rotation patterns to which a sample of interest can be compared to deduce molecular orientation and clustering. By simulating patterns for other molecular orientations, we have confirmed that the match between experimental and simulated EPR rotation patterns is not a fortuitous coincidence; see Supporting Information for details. Furthermore, we find that (a) films grown on the same type of substrate have the same shape of EPR rotation pattern, irrespective of the CuPc concentration or thickness of film, and (b) films with the same CuPc concentration have similar line width, regardless of the substrate or thickness of film.

Comparing the contour maps for the CuPc:$C_{60}$ films shown in Figure 3 with those for CuPc:$H_2$Pc mixtures in Figure 4, it is evident that these films do not resemble either 50% CuPc:$H_2$Pc film. Rather, the CuPc:$C_{60}$ mixed films most closely resemble the 100% CuPc nontemplated film. The conclusion is that, in the co-deposited films of CuPc and $C_{60}$, the CuPc forms clusters with the molecular plane approximately perpendicular to the substrate. The improvement in solar cell efficiency upon blending with $C_{60}$ is, therefore, not the result of any change in molecular orientation but rather is due to an increased interface between donor and acceptor. Furthermore, the EPR data shown in Figure 3 demonstrates that the use of an intermediate layer of $H_2$Pc, which is known to improve open-circuit voltage in cells containing blended CuPc:$C_{60}$ active layers,[8,13] does not influence molecular orientation.

As we have seen above, the EPR line width yields information about whether the electron spins are randomly distributed or clustered; Figure 5a,b shows spectra of nontemplated and templated CuPc:$H_2$Pc films with the films orientated perpendicular to the magnetic field for varying stoichiometries. The increased

line width of the copper hyperfine structure from 5 to 75% spin concentration is assigned to dipolar broadening, the influence of fluctuating nearby magnetic dipoles on the measured spin. As the CuPc concentration increases further to 100%, exchange dominates and causes a narrowing of the spectrum. Although density functional theory provides an effective means of calculating the exchange,[28,29] the results are sensitive to the molecular packing and depend on the choice of exchange correlation functional. Our purpose here is not to model the exchange but rather to demonstrate how the concentration-dependent line width may be used as an indicator of clustering.

The visual comparison of model films and CuPc:$C_{60}$ provides us with a qualitative understanding of the nanostructure and texture of the CuPc:$C_{60}$ films but does not yield quantitative results. Without validation, these conclusions would be highly suggestive but not definitive. To provide this validation, we consider the EPR of crystalline thin films where, in contrast to the amorphous solar cell films, XRD can provide useful information. The comparison of EPR and XRD on the same film allows us to robustly connect our EPR results with the historical literature that has primarily focused on XRD analysis.

For this comparison, we chose to use the 5% CuPc:$H_2$Pc film as it contains contributions from nitrogen and copper hyperfine couplings both of which have an angular dependence. The rotation patterns of nontemplated and templated 5% CuPc:$H_2$Pc films are depicted in Figure 5c,d, respectively. The peak at ~350 mT is assigned to the summation of an oxygen-derived free radical in $H_2$Pc,[30] and a signal from the Kapton film that does not change position as the angle, $\tau$, between the normal to the substrate and the magnetic field is varied in contrast to the strong dependence observed for the CuPc transitions. In the templated film, the largest hyperfine splitting is observed at $\tau \sim 0°$ since the plane of the molecule is approximately parallel to the substrate, whereas in the nontemplated film, it occurs at $\tau \sim 90°$. As a guide to the eye, the angular variation of the *g*-factor and Cu hyperfine coupling is plotted in red, with the simulated molecular orientation chosen to represent either a templated film (at $\tau = 0°$, the angle between the normal to the molecular plane and *B*-field was set to 0°) or nontemplated film (at $\tau = 0°$, the same angle was set to 90°).

The EPR rotation patterns can be compared to the XRD scans in Figure 6a,b that show that diluted CuPc thin films adopt the same α-phase as their pristine equivalents,[31] whose structure has recently been redetermined.[32] However, the systematic absences of peaks compared to those observed in a fully randomly oriented powder indicate that the crystallites in the films display a preferential orientation with respect to the substrate (*i.e.*, are textured). Note that the contribution from the PTCDA layer to the XRD of the templated films is small.

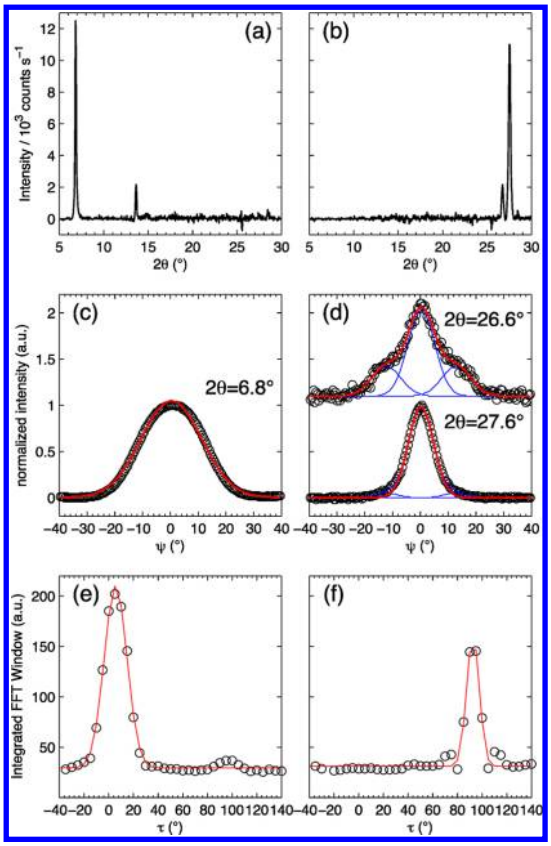


**Figure 6. XRD patterns of thin films deposited on Kapton, (a) 5% CuPc:$H_2$Pc and (b) templated 5% CuPc:$H_2$Pc. The diffraction planes in (a) are (100) and (200) for α-CuPc at 6.8 and 13.7°, respectively, and in (b) are (01−2) of α-CuPc at 26.6°, (11−2) of α-CuPc at 27.6°, and (01−2) for β-PTCDA at 27.6°; $\psi$ curves (circles) and Gaussian fits (red lines) for (c) 5% CuPc film at $2\theta = 6.8°$ and (d) templated 5% CuPc:$H_2$Pc film at $2\theta = 26.6°$ (top) and $2\theta = 27.6°$ (bottom). The Kapton background has been removed, and the intensity has been normalized to the central peak. Plots of the variation of the "sharpness measure" with angle $\tau$ for (e) nontemplated and (f) templated films and Gaussian fits.**

To determine the orientation of the diffracting planes, we acquire $\psi$ curves, where the intensity of a particular XRD reflection is recorded as the sample is tilted by an angle $\psi$ about an axis at the intersection of the substrate and the plane formed by the X-ray beam path. Figure 6c shows the $\psi$ curves of the nontemplated 5%CuPc:$H_2$Pc film at $2\theta = 6.8°$ (arising from diffraction from the (100) planes[32]). The intensity peaks at $\psi = 0°$ implying that the (100) plane is preferentially parallel to the substrate and the molecules form an angle of 82° with it; the molecular orientation with respect to the crystallographic planes is deduced from analysis of the α-CuPc crystal structure.[32] Figure 6d depicts the $\psi$ curve of the templated 5%CuPc:$H_2$Pc film at $2\theta = 26.6$ and 27.6° (due to diffraction from the (01−2) and (11−2) planes of the α-phase, respectively[32]). The presence of two satellite peaks indicates that the grains adopt two orientations, with the

$2\theta$ plane preferentially parallel or tilted 12° to the substrate. This difference is close to 14.5°, the angular separation between the (01−2) and (11−2) planes and further confirms that these two planes are preferentially parallel to the substrate in different grains. This differs from previous interpretations[4,5,7,22,33] which mainly relied on $\theta-2\theta$ XRD, and crucially also used a crystal structure that has been questioned by Hoshino *et al.*[32] We believe that the present interpretation relies on more robust experimental evidence including the use of pole figures; it utilizes an arguably more accurate crystal structure[32] and addresses the issues raised by previous research. Our model defines molecular planes tilted at angles of 7.5 and 9.0° with respect to the substrate.

The widths of the $\psi$ curves as obtained from the Gaussian fitting are larger for the nontemplated films ($\sigma = 11°$) than for the templated films ($\sigma = 5°$ for both the central and satellite peaks), as the stronger interactions with the PTCDA layer constrain the CuPc crystallite orientation more forcefully than the Kapton substrate alone.

To extract the spread of molecular orientations from the EPR data, a windowed Fourier transform is used to obtain an empirical "sharpness measure" that quantifies the resolvability of the nitrogen hyperfine structure. Three effects contribute to this sharpness measure: the variation with angle of the *g*-factor and the hyperfine coupling, the natural line width and its variation with angle, and the distribution of molecular orientations. The sharpness measure peaks when the film is oriented so that there is minimum angular variation in the effective *g*-factors and hyperfine couplings; this happens when large populations of molecules lie with the principal axes of the *g* and *A* tensors aligned with the field. In these films, this occurs at the orientations $\tau = 0°$ and $\tau = 90°$ for the nontemplated and templated cases, respectively.

Plots of the windowed Fourier transform *versus* rotation angle are shown in Figure 6e,f. The peak locations confirm the inference from the spectra of Figure 5c,d that the dominant orientation is with the molecular *z*-axes almost in-plane for the nontemplated films and almost perpendicular for templated films. The peak widths ($\sigma = 9°$ for the nontemplated and $\sigma = 5°$ for the templated films) provide a measure of the spread of molecular orientations (see Supporting Information for details) and can be directly compared to the mosaicities ($\sigma = 11°$ and $\sigma = 5°$, respectively) determined by XRD, with which they are found to match well.

## DISCUSSION

We have presented a fingerprinting technique for determining both molecular orientation and clustering in films of CuPc based on EPR spectroscopy. Although determination of the orientation of crystallographic planes may be achieved by XRD, molecular orientation can only be extracted when there is a sufficiently large number of visible Bragg peaks to determine how the molecules are situated within the crystallographic unit cell. In contrast, EPR measures the molecular orientation directly, through the anisotropy of the electronic Zeeman and hyperfine interactions that are characteristic of the molecule itself—the method is therefore applicable to poor crystals and even noncrystalline samples. Furthermore, EPR allows clustering to be identified *via* the effect of spin−spin interactions on the line width. In this paper, we have validated the EPR approach through spectral simulation and comparison with XRD data on crystalline films. In a test case, important for understanding the efficiency of solar cells, where no information is available from XRD, we demonstrate that the CuPc forms clusters in CuPc:$C_{60}$ mixed films with the molecular planes of the Pc molecules oriented perpendicular to the substrate.

The CuPc cluster size is not measured explicitly, but our data imply considerable constraints. The EPR measurements impart a lower bound since the CuPc:$C_{60}$ film spectra (shown in Figure 2c,d) show no sign of hyperfine splitting. This suggests that each CuPc molecule is in a cluster two or more molecules thick along their stacking direction. The corresponding X-ray data contain no trace of diffraction, and because clusters above ~10 nm would lead to a diffraction signal, the upper bound for the cluster size is on the order of 26 molecules along the one-dimensional columns. The clusters therefore are small regions within the morphology visible by AFM, which consists of spherical features with a characteristic length scale on the order of 50 nm, corresponding to ~130 molecules stacked along one-dimensional columns.

We conclude that in today's "optimal" blended Pc-based solar cells, the Pc molecules are not oriented in the ideal direction for charge transport. This implies that improved solar cells could be manufactured by combining blending with engineering of molecular orientation in order to rotate the CuPc molecular planes parallel to the substrate and optimize the degree of clustering. Our fingerprinting approach facilitates the required film growth studies because now the relevant microscopic detail is accessible. The technique is not limited to CuPc samples but can be used to study molecular orientation and clustering in other anisotropic spin-bearing species. With suitable optical excitation, inducing paramagnetic excited states,[34] EPR even has the potential to be extended to measurements on samples with diamagnetic ground states. Furthermore, the technique is convenient and low-cost compared to electron microscopy and synchrotron-based methods. As our measurements could be performed on a single sheet of film (see Supporting Information), and EPR has been demonstrated to be

compatible with the study of organic devices,[35] the technique could be implemented for quality control in a roll-to-roll fabrication plant of flexible solar cells or displays using a simple Fabry–Perot EPR resonator.

## MATERIALS AND METHODS

The films were grown by organic molecular beam deposition (OMBD) in a Kurt J. Lesker Spectros system with a base pressure of around $5 \times 10^{-7}$ mbar on flexible 25 $\mu$m thick Kapton substrates at a combined deposition rate of 1 Å/s. Two different versions of each film were produced: (1) deposited directly on the Kapton and (2) on a 20 nm intermediate layer of PTCDA or $H_2Pc$ for the Pc and CuPc:$C_{60}$ films, respectively. The proportion of materials in mixed films is quoted in percentage by mass. The intermediate layer was deposited in the same chamber without breaking the vacuum at a rate of 0.2 Å/ s.

The XRD $\theta/2\theta$ patterns were obtained using a Panalytical X'Pert PRO MPD with Ni filtered Cu $K_\alpha$ radiation from a fixed anode at 40 kV, 40 mA. Data were collected within the range $5° < 2\theta < 30°$ with a 0.033° step size, with a counting time of 8 s per point in all cases. The Kapton substrate with films deposited on it was cut into ~1 cm × 1 cm samples. The $\psi$ curves were obtained using a Panalytical X'Pert MRD with Ni filtered Cu $K_\alpha$ radiation at 40 kV and 40 mA. Data were collected within the range $-40° < \psi < 40°$ with a 0.5° step size at the stated $2\theta$. The Kapton substrate with the film deposited on it was cut into ~5 cm × 2 cm strips and mounted with the long axis parallel to the source detector axis.

The AFM measurements were performed on a Veeco Dimension 3100 microscope in tapping mode, using silicon tips supplied by MicroMasch.

EPR spectra were collected using a Bruker EMX Plus X-band spectrometer equipped with a 4122SHQE resonator operating at a frequency of approximately 9.8 GHz. A 30 mm × 10 mm piece of the Kapton substrate with the film deposited on it was cut into 10 strips which were placed inside a sample tube between two pieces of a quartz rod split down the middle, holding the films flat and parallel. The tube was held in a goniometer, allowing rotation of the sample within the resonator thus changing the angle $\tau$ (see Figures 2–5), between the magnetic field and the film. EPR spectra were recorded in the dark with a 5° step size for the 5%CuPc:$H_2Pc$ films and a 10° step size for the 50% CuPc:$H_2Pc$, 100% CuPc and CuPc:$C_{60}$ films for at least 220°. For comparison, EPR spectra were also recorded in the same resonator with a single sheet of CuPc:$C_{60}$ (area 5.6 cm × 0.8 cm). The spectra (shown in the Supporting Information) reproduce the angular dependence found with the stacked sheets, but with lower sensitivity due to the non-optimal resonator geometry.

The sharpness measure is found by an empirical procedure: an appropriate portion of the EPR spectrum is selected by performing a Gaussian wavelet Fourier transform (blue vertical lines in 5c and 5d designate two standard deviations). The Gaussian cutoff is chosen to prevent artifacts from an abrupt termination; the center was at 341 mT and standard deviation was 5 mT, but the qualitative results remain over a range of parameters. The sharpness measure is derived by integrating the Fourier transform over a small range of frequencies around that corresponding to the nitrogen hyperfine splitting.

In the EPR simulations, we take into account the important elements in the experiments, such as the nearest-neighbor exchange interaction, the Cu hyperfine coupling, and the Zeeman energy in the spin Hamiltonian

$$\hat{H} = J\vec{S}_1 \cdot \vec{S}_2 + \vec{S}_1 \cdot \vec{\vec{A}}_{Cu} \cdot \vec{I}_1^{Cu} + \vec{S}_2 \cdot \vec{\vec{A}}_{Cu} \cdot \vec{I}_2^{Cu} + \mu_B \vec{B} \cdot \vec{\vec{g}}_e \cdot (\vec{S}_1 + \vec{S}_2) + \mu_N g_n \vec{B} \cdot (\vec{I}_1^{Cu} + \vec{I}_2^{Cu})$$

Here $J$ is the exchange coupling between neighboring Cu electron spins $\vec{\vec{A}} = \begin{pmatrix} A_\perp & & \\ & A_\perp & \\ & & A_\parallel \end{pmatrix}$ is the tensor for anisotropic hyperfine coupling with $A_\perp = -83$ MHz, $A_\parallel = -648$ MHz and $\vec{\vec{g}}_e = \begin{pmatrix} g_\perp & & \\ & g_\perp & \\ & & g_\parallel \end{pmatrix}$ is the anisotropic $g$-tensor with $g_\perp = 2.0390$, $g_\parallel = 2.1577$.[25] We first compute EPR spectra by Fermi's Golden Rule, assuming a Gaussian homogeneous line broadening, for a range of relative orientations of the static magnetic field and the molecular orientation. Then in order to describe the realistic orientation distribution of CuPc, we assume a Gaussian distribution for $\rho$, the angle between the molecular $z$-axis and the normal to the plane ($\overline{\rho}_{templated,1} = 7°$, $\overline{\rho}_{templated,2} = 9°$, $\sigma_{templated} = 3.82°$, $\overline{\rho}_{nontemplated} = 82°$, $\sigma_{templated} = 11.04°$), and a uniform distribution in the film plane based on XRD patterns. Using this information, we perform an angular averaging with open Plate-Carré spherical codes[36] for $\rho$ and $\tau$. We select the $\rho$ angle from $\overline{\rho} - 3\sigma_\rho$ to $\overline{\rho} + 3\sigma_\rho$ with interval $\sigma_\rho$ and $\tau$ from 0 to 360° with a 6° interval, yielding a total of 847 points on the sphere. The line broadening is set to be 150 MHz to take into account the effect of further splitting due to nitrogen hyperfine couplings. In all, nine simulations have been performed to support the experimental results. Four simulations were done for a templated molecular and a nontemplated pair with and without exchange interaction (we consider $J = 1$ K, equivalent to 21 GHz), as shown in Figure 4. Another four simulations were performed for $\overline{\rho} = 16°$ and $\overline{\rho} = 64°$ with the same deviations to illustrate the sensitivity of the EPR spectra to the molecular orientations (see Supporting Information). A powder spectrum, where both $\rho$ and $\tau$ are uniformly distributed, was also simulated (see Supporting Information).

*Conflict of Interest:* The authors declare no competing financial interest.

*Acknowledgment.* We thank the Research Council UK and the Engineering and Physical Sciences Research Council (EPSRC) for financial support through the Basic Technology Grant "Molecular Spintronics". We thank Professor David W. McComb for useful discussions, and Mr Richard Sweeney for assistance with the diffraction measurements.

*Supporting Information Available:* Additional experimental details and figures. This material is available free of charge *via* the Internet at http://pubs.acs.org.

## REFERENCES AND NOTES

1. Dimitrakopoulos, C. D.; Malenfant, P. R. L. Organic Thin Film Transistors for Large Area Electronics. *Adv. Mater.* **2002**, *14*, 99–117.
2. Sirringhaus, H.; Brown, P. J.; Friend, R. H.; Nielsen, M. M.; Bechgaard, K.; Langeveld-Voss, B. M. W.; Spiering, A. J. H.; Janssen, R. A. J.; Meijer, E. W.; Herwig, P.; *et al.* Two-Dimensional Charge Transport in Self-Organized, High-Mobility Conjugated Polymers. *Nature* **1999**, *401*, 685–688.
3. Manaka, T.; Taguchi, K.; Ishikawa, K.; Takezoe, H. Highly Aligned α-Type Copper Phthalocyanine Formed on Rubbed Polyimide Alignment Layer. *Jpn. J. Appl. Phys.* **2000**, *39*, 4910–4911.
4. Heutz, S.; Cloots, R.; Jones, T. S. Structural Templating Effects in Molecular Heterostructures Grown by Organic Molecular-Beam Deposition. *Appl. Phys. Lett.* **2000**, *77*, 3938–3940.
5. Heutz, S.; Jones, T. S. Structural and Morphological Modifications in Double Layer Heterostructures Containing $H_2Pc$, Perylene-3,4,9,10-Tetracarboxylic Dianhydride and $Alq_3$. *J. Appl. Phys.* **2002**, *92*, 3039–3046.
6. Sullivan, P.; Jones, T. S.; Ferguson, A. J.; Heutz, S. Structural Templating as a Route to Improved Photovoltaic Performance in Copper Phthalocyanine/Fullerene ($C_{60}$) Heterojunctions. *Appl. Phys. Lett.* **2007**, *91*, 233114–233113.

7. Lassiter, B. E.; Lunt, R. R.; Renshaw, C. K.; Forrest, S. R. Structural Templating of Multiple Polycrystalline Layers in Organic Photovoltaic Cells. *Opt. Express* **2010**, *18*, A444–A450.
8. Heutz, S.; Sullivan, P.; Sanderson, B. M.; Schultes, S. M.; Jones, T. S. Influence of Molecular Architecture and Intermixing on the Photovoltaic, Morphological and Spectroscopic Properties of CuPc-$C_{60}$ Heterojunctions. *Sol. Energy Mater. Sol. Cells* **2004**, *83*, 229–245.
9. Xue, J. G.; Rand, B. P.; Uchida, S.; Forrest, S. R. Mixed Donor−Acceptor Molecular Heterojunctions for Photovoltaic Applications. II. Device Performance. *J. Appl. Phys.* **2005**, 98.
10. Opitz, A.; Wagner, J.; Bruetting, W.; Hinderhofer, A.; Schreiber, F. Molecular Semiconductor Blends: Microstructure, Charge Carrier Transport, and Application in Photovoltaic Cells. *Phys. Status Solidi A* **2009**, *206*, 2683–2694.
11. Xue, J. G.; Uchida, S.; Rand, B. P.; Forrest, S. R. Asymmetric Tandem Organic Photovoltaic Cells with Hybrid Planar-Mixed Molecular Heterojunctions. *Appl. Phys. Lett.* **2004**, *85*, 5757–5759.
12. Hsiao, Y.-S.; Whang, W.-T.; Suen, S.-C.; Shiu, J.-Y.; Chen, C.-P. Morphological Control of Cupc and Its Application in Organic Solar Cells. *Nanotechnology* **2008**, *19*, 415603.
13. Sullivan, P.; Heutz, S.; Schultes, S. M.; Jones, T. S. Influence of Codeposition on the Performance of CuPc-$C_{60}$ Heterojunction Photovoltaic Devices. *Appl. Phys. Lett.* **2004**, *84*, 1210–1212.
14. Rand, B. P.; Xue, J. G.; Uchida, S.; Forrest, S. R. Mixed Donor−Acceptor Molecular Heterojunctions for Photovoltaic Applications. I. Material Properties. *J. Appl. Phys.* **2005**, *98*, 124902.
15. Peisert, H.; Schwieger, T.; Auerhammer, J. M.; Knupfer, M.; Golden, M. S.; Fink, J.; Bressler, P. R.; Mast, M. Order on Disorder: Copper Phthalocyanine Thin Films on Technical Substrates. *J. Appl. Phys.* **2001**, *90*, 466–469.
16. Chen, W.; Huang, H.; Chen, S.; Huang, Y. L.; Gao, X. Y.; Wee, A. T. S. Molecular Orientation-Dependent Ionization Potential of Organic Thin Films. *Chem. Mater.* **2008**, *20*, 7017–7021.
17. Collins, B. A.; Cochran, J. E.; Yan, H.; Gann, E.; Hub, C.; Fink, R.; Wang, C.; Schuettfort, T.; McNeill, C. R.; Chabinyc, M. L.; *et al.* Polarized X-ray Scattering Reveals Non-crystalline Orientational Ordering in Organic Films. *Nat. Mater.* **2012**, *11*, 536–543.
18. Basova, T. V.; Kolesov, B. A. Raman Polarization Studies of the Orientation of Molecular Thin Films. *Thin Solid Films* **1998**, *325*, 140–144.
19. Bräuer, B.; Fronk, M.; Lehmann, D.; Zahn, D. R. T.; Salvan, G. Magneto-Optical Kerr Effect Spectroscopy—A Sensitive Tool for Investigating the Molecular Orientation in Organic Semiconductor Films. *J. Phys. Chem. B* **2009**, *113*, 14957–14961.
20. Aguirre, A.; Gast, P.; Orlinskii, S.; Akimoto, I.; Groenen, E. J. J.; El Mkami, H.; Goovaerts, E.; Van Doorslaer, S.; Multifrequency, E. P. R. Analysis of the Positive Polaron in $I_2$-Doped Poly(3-hexylthiophene) and in Poly-2-methoxy-5-(3,7-dimethyloctyloxy)-1,4-phenylenevinylene. *Phys. Chem. Chem. Phys.* **2008**, *10*, 7129–7138.
21. Marumoto, K.; Nagano, Y.; Sakamoto, T.; Ukai, S.; Ito, H.; Kuroda, S. ESR Studies of Field-Induced Polarons in MIS Diode Structures with Self-Organized Regioregular Poly(3-hexylthiophene). *Colloids Surf., A* **2006**, *284*, 617–622.
22. Sugiyama, K.; Iizuka, S.; Yashir, H.; Fukuda, H.; Shimoyama, Y. Molecular Orientation and Electromagnetic Properties of Perhydrogenated and Perfluorinated Copper Phthalocyanine Thin Films. *Jpn. J. Appl. Phys.* **2008**, *47*, 492–495.
23. Ingram, D. J. E.; Bennett, J. E. Paramagnetic Resonance in Phthalocyanine, Chlorophyll and Haemoglobin Derivatives. *J. Chem. Phys.* **1954**, *22*, 1136–1137.
24. Bennett, J. E.; Ingram, D. J. E. Paramagnetic Resonance in Copper Phthalocyanine. *Nature* **1955**, *175*, 130–131.
25. Finazzo, C.; Calle, C.; Stoll, S.; Van Doorslaer, S.; Schweiger, A. Matrix Effects on Copper(II)Phthalocyanine Complexes. A Combined Continuous Wave and Pulse EPR and DFT Study. *Phys. Chem. Chem. Phys.* **2006**, *8*, 1942–1953.
26. Van Vleck, J. H. The Dipolar Broadening of Magnetic Resonance Lines in Crystals. *Phys. Rev.* **1948**, *74*, 1168–1183.
27. Anderson, P. W.; Weiss, P. R. Exchange Narrowing in Paramagnetic Resonance. *Rev. Mod. Phys.* **1953**, *25*, 269–276.
28. Heutz, S.; Mitra, C.; Wu, W.; Fisher, A. J.; Kerridge, A.; Stoneham, M.; Harker, T. H.; Gardener, J.; Tseng, H. H.; Jones, T. S.; *et al.* Molecular Thin Films: A New Type of Magnetic Switch. *Adv. Mater.* **2007**, *19*, 3618–3622.
29. Wu, W.; Kerridge, A.; Harker, A. H.; Fisher, A. J. Structure-Dependent Exchange in the Organic Magnets Cu(II)Pc and Mn(II)Pc. *Phys. Rev. B* **2008**, *77*, 184403.
30. Assour, J. M.; Harrison, S. E. On the Origin of Unpaired Electrons in Metal-Free Phthalocyanine. *J. Phys. Chem.* **1964**, *68*, 872–876.
31. Lucia, E. A.; Verderame, F. D. Spectra of Polycrystalline Phthalocyanines in the Visible Region. *J. Chem. Phys.* **1968**, *48*, 2674–2681.
32. Hoshino, A.; Takenaka, Y.; Miyaji, H. Redetermination of the Crystal Structure of α-Copper Phthalocyanine Grown on KCl. *Acta Crystallogr., Sect. B* **2003**, *59*, 393–403.
33. Sakurai, T.; Fukasawa, R.; Kawai, S.; Akimoto, K. Structural and Optical Properties of Phthalocyanine Thin Films Grown on Glass with 3,4,9,10-Perylene Tetracarboxylic Dianhydride Intermediate Layer. *Jpn. J. Appl. Phys.* **2006**, *45*, 397–400.
34. Kay, C. W. M.; Di Valentin, M.; Möbius, K. Time-Resolved EPR and Endor Study of the Photoexcited Triplet State of Free-Base Tetraphenylchlorin in a Crystalline Toluene Matrix. *J. Chem. Soc., Perkin Trans. 2* **1997**, 2563–2568.
35. Lupton, J. M.; McCamey, D. R.; Boehme, C. Coherent Spin Manipulation in Molecular Semiconductors: Getting a Handle on Organic Spintronics. *ChemPhysChem* **2010**, *11*, 3040–3058.
36. Ponti, A. Simulation of Magnetic Resonance Static Powder Lineshapes: A Quantitative Assessment of Spherical Codes. *J. Magn. Reson.* **1999**, *138*, 288–297.